



1 **A dataset of microclimate and radiation and energy fluxes from the Lake Taihu Eddy**

2 **Flux Network**

3 Zheng Zhang^{a,b}, Mi Zhang^{a,b,d}, Chang Cao^{a,b}, Wei Wang^{a,b}, Wei Xiao^{a,b,d}, Chengyu Xie^{a,b},
4 Haoran Chu^{a,b}, Jiao Wang^{a,b}, Jiayu Zhao^{a,b}, Lei Jia^{a,b}, Qiang Liu^{a,b}, Wenjing Huang^{a,b},
5 Wenqing Zhang^{a,b}, Yang Lu^{a,b}, Yanhong Xie^{a,b}, Yi Wang^{a,b}, Yini Pu^{a,b}, Yongbo Hu^{a,b}, Zheng
6 Chen^{a,b}, Zhihao Qin^{a,b}, Xuhui Lee^{c*}

7

8 a Yale-NUIST Center on Atmospheric Environment, International Joint Laboratory on
9 Climate and Environment Change (ILCEC), Nanjing University of Information Science and
10 Technology, Nanjing, Jiangsu Province, China

11

12 b Key Laboratory of Meteorological Disaster, Ministry of Education and Collaborative
13 Innovation Center on Forecast and Evaluation of Meteorological Disasters, Nanjing
14 University of Information Science and Technology, Nanjing, Jiangsu Province, China

15

16 c School of Forestry and Environmental Studies, Yale University, New Haven, CT, USA

17

18 d NUIST-Wuxi Research Institute, Wuxi, Jiangsu Province, China

19 * Corresponding author: xuhui.lee@yale.edu

20



21 **Abstract**

22 Eddy covariance data are widely used for the investigation of surface-air interactions.
23 Although numerical datasets exist in public depositories for upland ecosystems, few research
24 groups have released eddy covariance data collected over lakes. In this paper, we describe a
25 dataset from the Lake Taihu Eddy Flux Network, a network consisting of seven lake sites and
26 one land site. Lake Taihu is the third largest freshwater lake (area 2,400 km²) in China, under
27 the influence of subtropical climate. The dataset spans the period from June 2010 to
28 December 2018. Data variables are recorded at half-hourly intervals and include
29 micrometeorology (air temperature, humidity, wind speed, wind direction, rainfall, and
30 water/soil temperature profile), the four components of surface radiation balance, friction
31 velocity, and sensible and latent heat fluxes. Except for rainfall and wind direction, all other
32 variables are gap-filled, with each datapoint marked by a quality flag. Several areas of
33 research can potentially benefit from the publication of this dataset, including evaluation of
34 mesoscale weather forecast models, development of lake-air flux parameterizations,
35 investigation of climatic controls on lake evaporation, validation of remote sensing surface
36 data products, and global synthesis on lake-air interactions. The dataset is publicly available
37 at <https://yncenter.sites.yale.edu/data-access> and from Harvard Dataverse
38 <https://doi.org/10.7910/DVN/HEWCWM> (Zhang et al., 2020)

39

40



41 **1. Introduction**

42 Inland lakes and reservoirs are a vital freshwater resource for the society. Globally, there are
43 more than 27 million water bodies with size greater than 0.01 km², occupying a total of 3.5%
44 of the Earth's land surface area (Downing et al., 2006; Verpoorter et al., 2014). Accurate
45 observation of the lake microclimate and lake-air interactions will help to better manage this
46 water resource and to better predict how it may be affected by environmental changes.
47 Towards that end, an increasing number of studies have deployed the eddy covariance (EC)
48 methodology to monitor physical state (temperature, wind, humidity) and process variables
49 (momentum flux, and radiation and energy fluxes) in the lake environment (Vesala et al.,
50 2006; Blanken et al., 2011; Nordbo et al., 2011; Wang et al., 2014; Li et al., 2015; Yusup and
51 Liu, 2016; Du et al., 2018; Hamdani et al., 2018; Xiao et al., 2018; Wang et al., 2019). Unlike
52 EC studies in upland ecosystems, however, data from these lake studies are rarely published
53 as data papers or are archived in public data depositories accessible by the broader scientific
54 community. For example, of the nearly 500 sites that have contributed EC and
55 micrometeorological data to AmeriFlux, a public data depository
56 (<https://ameriflux.lbl.gov/data/data-availability/>), none is a lake site. Although a few
57 scientific groups have provided data supplements to their scientific papers on lake-air fluxes
58 (e. g., Charusombat et al., 2018; Franz et al., 2018; Zhao and Liu, 2018), we are not aware of
59 a data paper devoted to systematic description and archival of EC lake observations.

60

61 In this paper, we describe the dataset from the Lake Taihu Eddy Flux Network (Lee et al.,
62 2014). Established in 2010, the network currently consists of six active lake sites, one



63 inactive lake site, and one active land site. Lake Taihu is the third largest freshwater lake
64 (area 2,400 km²) in China. Data variables are recorded at half-hourly intervals and the
65 measurement has continued for over eight years. Several areas of research can potentially
66 benefit from the publication of this dataset, including evaluation of mesoscale weather
67 forecast models, development of lake-air flux parameterizations, investigation of climatic
68 controls on lake evaporation, validation of remote sensing surface data products, and global
69 synthesis on lake-air interactions.

70

71 This paper is organized as follows. Section 2 is a brief overview of the sites and the
72 instruments used by the network. This is followed, in Section 3, with a description of data
73 quality measures deployed during the field monitoring. Section 4 provides the essential
74 information about the dataset, including data variables, gap-filling methods, and data quality
75 flags. Results of post-field evaluation of the data quality are given in Section 5.

76

77 Users of this dataset may be interested in the relevant papers published by our group. Lee et
78 al. (2014) gave an overview of the Lake Taihu Eddy Flux Network. Using the data collected
79 at a subset of the sites and during the early phase of the network, Wang et al. (2014)
80 investigated the spatial variability of energy and momentum fluxes across the lake. Xiao et al.
81 (2013) improved the bulk parameterizations of heat, water and momentum fluxes for shallow
82 lakes. Deng et al. (2013) and Hu et al. (2017) modified the CLM lake simulator (Subin et al.,
83 2012) to improve its prediction of the lake evaporation. Wang et al. (2017) and Zhang et al.
84 (2019b) evaluated the performance of two mesoscale models of the lake-land breeze. More



85 recently, Xiao et al. (2020, manuscript in review) investigated drivers of the interannual
86 variability of the lake evaporation observed at one of the lake sites (BFG). The value of the
87 dataset is enhanced by these peer-reviewed publications because they have helped us to
88 continuously improve our measurement and data processing protocols. For example, we have
89 used the locally-calibrated bulk parameterizations of Xiao et al. (2013) to gap-fill the flux
90 variables.

91

92 **2. Sites and Instrumentation**

93 **2.1 Sites and data periods**

94 Table 1 shows the basic site information and Figure 1 is a map that gives the relative position
95 of Lake Taihu in China and locations of the EC measurement sites. Also shown in Figure 1
96 are WMO baseline weather stations around the lake, whose data can be obtained from
97 National Meteorological Information Center in China (<http://data.cma.cn/site/index.html>).
98 The lake, located between the latitudinal range of 30°5'40" N to 31°32'58" N and
99 longitudinal range of 119°52'32" E to 120°36'10" E, has a total area of 2400 km² and an
100 average depth of 1.9 m. The climate is subtropical monsoon, with an annual mean
101 temperature of 16.2°C and annual total precipitation of 1122 mm. The lake is ice-free
102 throughout the year.

103

104 The EC network consists of seven lake sites and one land site. The lake sites (Meiliangwan
105 (MLW), Dapukou (DPK), Bifenggang (BFG), Xiaoleishan (XLS), Pingtaishan (PTS),
106 Dongtaihu (DTH), Meiliangwan2 (MLW2)) are distributed according to biological



107 characteristics and across eutrophication gradients of the lake. The MLW site, located in
108 Meiliangwan Bay near the north shore of Lake Taihu, was the first site in operation; the
109 measurement began in June 2010 and was replaced by MLW2 in 2018, at 10 km southwest of
110 MLW. Both MLW and MLW2 sites are located in the lake eutrophic zone. BFG is located in
111 the east part of Lake Taihu in relatively clean water inhabited by submerged vegetation with
112 a growth season from April to November. DTH is located in the shallow water (mean depth
113 of 1.3 m) in the southeast part of the lake. After more than 20 years of crab aquaculture, this
114 zone was returned to unmanaged state in December 2018 in order to improve water quality.
115 The observation at DTH enables the examination of lake-air exchange processes in the
116 transition from human management to a natural state. PTS is situated in the middle of Lake
117 Taihu where occasional algal blooms occur and no aquatic vegetation is present. DPK is
118 located near the west shore, in a relatively deep (depth 2.5 m) super eutrophic zone due to
119 heavy influence of agricultural and urban runoffs. XLS is located in the relatively clean and
120 vegetation-free zone in the southeast. Finally, DS is a land site surrounded by rice agriculture,
121 serving as a land reference for the lake sites. The MLW site is situated at a distance of 200 m
122 from the north shore of the lake. All the other lake sites in the lake are at a distance of more
123 than 1 km away from the land.

124

125 **2.2 Instrumentation**

126 Each site is equipped with an EC system for long-term, continuous monitoring of the surface
127 momentum, sensible heat, latent heat and carbon dioxide fluxes. The EC system consists of a
128 sonic anemometer/ thermometer (Model CSAT3A; Campbell Scientific, Logan, UT, USA)



129 and a CO₂/H₂O infrared analyzer (Model 7500A, LI-COR, Inc., Lincoln, NE, USA at DS,
130 MLW, MLW2 and DPK; Model EC150, Campbell Scientific at other sites). The EC
131 instrument is at a height of 3.5 to 20 m above the water or the soil surface. Other
132 measurements include air humidity and air temperature (Model HMP45D/HMP155A;
133 Vaisala, Inc, Helsinki, Finland), wind speed and wind direction (Model 03002; R. M. Young
134 Company, Traverse City, MI, USA) and four components of the net radiation (Model CNR4;
135 Kipp & Zonen B. V., Delft, the Netherlands). At the lake sites, water temperature profile was
136 measured with temperature probes (Model 109-L; Campbell Scientific) at the water depth of
137 20, 50, 100, and 150 cm and in the sediment at about 5 cm below bottom of the water column.
138 At the DS land site, soil temperature profile was measured with the same type of probes at
139 the depths of 5, 10, 20 cm. The MLW and the DS sites are supported by A/C power and other
140 sites are powered by battery packs connected to solar panels.

141

142 The methane flux was measured at MLW, BFG and DTH for selected periods, in addition to
143 the standard variables described above, using a flux-gradient system (at MLW; Xiao et al.
144 2014) and an open-path eddy covariance system (at BFG and DTH, Zhang et al., 2019a). The
145 carbon dioxide and methane flux data are not included in the current version of the data
146 release but will be added at a later time after the data quality has been fully examined and the
147 data gaps filled.

148

149 All the variables are reported as 30-min averages. The EC covariance data are expressed in
150 the natural coordinate system (Lee et al., 2004). Additionally, a small density correction has



151 been applied to the water vapor flux according to Webb et al. (1980).

152

153 **3 Data Quality Control during Field Monitoring**

154 Every site in the Lake Taihu Eddy Flux Network is equipped with a wireless transmission

155 module for real-time monitoring and for data transmission. Time series of all 30-min

156 variables are examined weekly and abnormal behaviors are flagged for site operators. Each

157 site is visited every one to two months to perform instrument repair and maintenance and to

158 download 10 Hz EC data. The data coverage rates are summarized in Table 2, where the

159 percentage values represent the proportions of data with quality flag 0 (Table 3).

160

161 The four-way net radiometers at MLW and XLS were compared in the field against a

162 laboratory standard of the same type in the summer of 2018 to check their long-term stability.

163 These two sites were chosen because they have been in operation for more than five years.

164 Additionally, the radiometer at MLW was relocated to MLW2 after MLW had been

165 discontinued. The laboratory standard, which had been calibrated at the manufacturer prior to

166 this performance evaluation, was mounted next to the field instrument for about 10 days at

167 each site, covering overcast to clear-sky conditions. The mean bias error was smaller than 1

168 W m^{-2} for all the radiation components. It was -0.81, -0.81, 0.79 and -0.44 W m^{-2} for the

169 downward shortwave, upward shortwave, downward longwave and upward longwave

170 radiation flux at MLW, respectively. The corresponding values were 0.91, 0.40, 0.69 and

171 0.77 W m^{-2} for XLS. (Comparison experiments are being planned for the other sites.)

172



173 The EC gas analyzers were calibrated every one to two years. The zero-point calibration was
174 carried out with high-purity nitrogen gas, the CO₂ span calibration was made with standard
175 carbon dioxide gases (in the concentration range of 389 to 525 ppm) provided by the National
176 Institute of Meteorology (NIM), China and certified to an accuracy of 1%, and the H₂O span
177 calibration was made with a portable dew-point generator (LI-610; LI-COR, Inc.).

178

179 **4. Gap-filling Methods and Data Quality Flags**

180 We use five-point moving average to screen outliers. If the deviation from the moving
181 average is greater than two standard deviations, the data point is discarded. If a gap length is
182 30 min to 1 h, the gap is filled by linear interpolation. Larger gaps in meteorological variables,
183 radiation components and water temperature are filled with linear regression involving
184 observation of the same variable at another site. This spatial interpolation consists of three
185 steps. First, linear correlation is calculated using the valid data at the target site and at all
186 other sites for the month during which the data gap occurred. Second, the observation at the
187 site with the highest linear correlation is used to establish a linear regression equation. Third,
188 the gap at the target site is filled with the linear regression and the observation at that site.

189

190 Radiation data gaps at the DS land site require special treatment. The radiometer at DS eddy
191 flux site ended in January 2013. Subsequent measurements of the radiation component are
192 provided by a radiometer belonging to the Dongshan WMO weather station at a distance of
193 50 m from the eddy covariance tower (Figure 1). While large gaps in meteorological
194 variables (air temperature, relative humidity, wind speed and air pressure), downward solar



195 radiation and downward longwave radiation are filled with the spatial interpolation method,
196 large gaps in upward shortwave radiation and upward longwave radiation cannot be filled
197 with data from other lake sites even with linear regression. In the case of the upward
198 shortwave radiation, the data gaps were filled using the relationship between downward
199 shortwave radiation and the monthly mean albedo. In the case of upward longwave radiation,
200 the data gaps were filled by a regression equation between the upward longwave radiation
201 and the fourth power of soil temperature at 5-cm depth. Compared to the original data, the
202 gap-filled data do not capture the full diurnal variations but the daily-mean upward shortwave
203 and longwave radiation fluxes seem reasonable.

204

205 Large data gaps in the EC variables (sensible heat flux, latent heat flux and friction velocity)
206 are filled with a hybrid method. If observations exist for the relevant state variable, the gap is
207 filled with the bulk transfer relationship using a locally-tuned transfer coefficient (Xiao et al.,
208 2013). For example, the relationship for filling gaps in the sensible heat flux is

$$209 \quad H = \rho_a c_p C_H U (T_s - T_a)$$

210 where ρ_a is air density, c_p is specific heat of air at constant pressure, C_H is the transfer
211 coefficient for sensible heat, T_a is air temperature and T_s is water surface temperature. If data
212 for the state variable is missing, the spatial interpolation method is used to fill the gaps in
213 these EC variables.

214

215 The spatial interpolation method described above occasionally causes a sudden jump at the
216 beginning or end of a data gap. To harmonize the data, we apply a 5-point moving averaging



217 to the gap-filled time series. If a data point deviates by 2 times of the standard deviation from
218 the moving average, it is replaced by linear interpolation using the two adjacent data points.

219

220 Each data point is assigned a quality flag to distinguish original measurements and gap-filled
221 values and gap-filling methods (Table 3). Flag 0 indicates high-quality original data. Other
222 flag values indicate gap-filled data or missing values. Flag 1 indicates that the data was filled
223 by temporal interpolation. Flag 2 indicates that the data was filled by the spatial interpolation
224 method. Flag 3 for the EC variables indicates that the data was filled by the bulk relationship.
225 We also use Flag 3 to mark the upward shortwave and longwave radiation data filled with the
226 albedo and the surface temperature relationship, respectively, for the DS land site. Missing
227 values occur on some situations, which are marked with Flag 4. Figure 3 is an example
228 showing the gap-filled time series of several variables at BFG along with the flag status.

229

230 Rainfall data has not been quantity-controlled or gap-filled. Because of the episodic nature of
231 rainstorms and high spatial variability of rainfall, it is not appropriate to fill data gaps with
232 the time or spatial interpolation method. The total rain amount is likely biased low because
233 no wind screens are used to protect the rain gages from the influence of wind which is much
234 higher on the lake than on land (Figure 4 below). On several site visits, the drain opening to
235 the tipping bucket was found to be partially blocked by debris. Rain amount at a constant and
236 low rate and excessively long rain duration are evidence of such blockage. The flag status of
237 0 for the rainfall variable simply indicates that the field measurement is available, but it does
238 not guarantee high data quality.



239

240 The data coverage begins from the start time of each site (Table 4) and the ends in December
241 2018. The time resolution is 30 min. The dataset includes microclimate variables (air pressure,
242 air temperature, relative humidity, wind speed, wind direction and rainfall), radiation fluxes
243 (upward and downward shortwave radiation, upward and downward longwave radiation),
244 water temperature at depth of 0.2 m, 0.5 m, 1.0 m and 1.5 m, and in the 5-cm sediment) and
245 eddy fluxes (friction velocity, and sensible heat and latent heat fluxes; Table 4). The time
246 stamp is Beijing time (UTC + 8 h) given by data columns 1 to 5 as year, month, day, hour,
247 and minute, and marks the end of the observation period. For example, time stamp “2012, 1,
248 12, 00” indicates that the data acquisition period is from 11:30 to 12:00 on January 1, 2012.

249

250 Although the data table does not include the radiative surface temperature T_s , the user can
251 easily calculate it from the two longwave radiation fluxes, as

252

$$T_s = \left(\frac{L_{\uparrow} - (1 - \varepsilon)L_{\downarrow}}{\varepsilon\sigma} \right)^{\frac{1}{4}}$$

253 where σ is the Stefan-Boltzmann constant, ε is emissivity, and L_{\uparrow} and L_{\downarrow} are upward and
254 downward longwave radiation flux, respectively. We use a value of 0.97 for lake surface
255 emissivity in this calculation (Deng et al., 2013; Wang et al., 2014).

256

257 **5. Data Consistency Evaluation**

258 Figure 4 compares the annual mean air temperature, relative humidity, and wind speed at the
259 Taihu eddy flux sites with those at the four WMO weather stations (Wuxi, Liyang, Huzhou



260 and Dongshan) around the lake (Figure 1). The error bars represent the maximum and
261 minimum values among the four WMO stations and the lines represent the mean values of
262 the four station measurements. The annual mean air temperature at DTH is 0.3°C higher than
263 the station mean. At other sites, air temperature is in close agreement of the weather station
264 data, in terms of both magnitude and inter-annual variability. The annual mean wind speed at
265 MLW, a site near the shoreline, is comparable with the station data. At other more exposed
266 sites, the wind speed is much higher than observed at the WMO stations. The annual mean
267 relative humidity RH shows a larger spread among the eddy flux sites than among the WMO
268 stations partly because the measurement height at the eddy flux sites is not standardized
269 (Table 1). The upward trends in RH over time at DPK and XLS seem to be related more to
270 aging of the sensor than to a real inter-annual variability. We have not fully investigated this
271 aging problem, but it is possible to rectify it by doing a detailed regression analysis against
272 the station data.

273

274 Consistency of the energy flux variables can be evaluated with the energy balance closure.
275 Using observations made at a subset of the sites in the earlier years of the flux network,
276 Wang et al. (2014) reported a closure rate of 70 % to 110 % on the monthly basis, meaning
277 that the sum of the measured monthly sensible and the latent heat flux $H + \lambda E$ is 70 % to
278 110 % of the monthly available energy $R_n - G$, where R_n net radiation and G is heat storage
279 in the water column. By selecting days without data gaps, we found that the daily energy
280 balance closure is in the range between 66 % and 78 % for all the lake sites and all the years.
281 Such closure rates are typical of eddy covariance observations (Tanny et al., 2008; Wilson et



282 al., 2002).

283

284 We have shown that the monthly latent heat flux at the lake sites MLW, BFG and DPK
285 during July 2010 to August 2012 follows the Priestley-Taylor (PT) model prediction with the
286 original PT constant α of 1.26 and that at the DS land site is in agreement with the PT model
287 if the constant is lowered to 1.0 (Lee et al., 2014). Figure 5 demonstrates that the same
288 relationships hold for all the sites and all the observational months, indicating the overall
289 stability of our measurement systems and the robustness of our gap-filling procedure. The
290 reader is reminded that the monthly latent heat flux in Figure 5 has been adjusted to force
291 energy closure following the method recommended by Barr et al. (1994), Blanken et al.
292 (1997) and Twine et al. (2000). (The half-hourly flux data in the data archive have not been
293 adjusted for energy balance.)

294

295 The Stefan-Boltzmann Law offers another way for checking data consistency. Because the
296 lake surface emits longwave radiation like a blackbody and because the annual mean air
297 temperature and the surface water temperature are nearly identical at this lake (Wang et al.,
298 2014), the change in the annual upward longwave radiation ΔL_{\uparrow} can be expressed as

$$299 \quad \Delta L_{\uparrow} = 4\sigma T_a^3 \Delta T_a$$

300 where T_a is annual mean air temperature, and Δ is the difference between the target year and
301 the year with the lowest air temperature observed at the site. All the five long-term lake sites
302 show good consistency between the longwave radiation and the air temperature observations
303 (Figure 6).



304

305 **6 Data availability**

306 All data can be open-accessed online for download and use at <https://yncenter.sites.yale.edu/>
307 and from Harvard Dataverse (<https://doi.org/10.7910/DVN/HEWCWM>, Zhang et al., 2020).

308

309 **7 Summary**

310 The dataset described here consists of microclimate variables (air temperature, air humidity,
311 wind speed, wind direction, water or soil temperature profile, and rainfall), four components
312 of the radiation balance, friction velocity, and sensible and latent heat fluxes observed at
313 seven lake sites and one land site. The period of coverage is from June 2018 to December
314 2018. The observation interval is 30 min. Except for rainfall and wind direction, all other
315 variables have been gap-filled. Every data point is tagged with a data quality flag to help the
316 user determine how to best use the data.

317

318 **Author contribution**

319 XL, WX and MZ directed the field program, ZZ performed data gap-filling and prepared the
320 data for public release, CC, WW, CX, HC, JW, JZ, LJ, QL, WH, WZ, YL, YX, YW, YP, YH,
321 ZC and ZQ participated in field data collection, and ZZ, XL and MZ wrote the manuscript.

322

323 **Competing interests**

324 The authors declare no conflict of interest.

325

326 **Acknowledgments**



327 This work was supported by the National Key R&D Program of China (2019YFA0607202),
328 the National Natural Science Foundation of China (grant numbers 41575147, 41801093, and
329 41475141) and the Priority Academic Program Development of Jiangsu Higher Education
330 Institutions (grand number PAPD).

331

332

333



334

335 **Table 1.** A list of sites in the Lake Taihu Eddy Flux Network

Site ID	MLW	DPK	BFG	XLS	PTS	MLW2	DTH	DS
Lat (°N)	31.4197	31.2661	31.1685	30.9972	31.2323	31.3818	31.0611	31.0799
Long (°E)	120.2139	119.9312	120.3972	120.1344	120.1086	120.1608	120.4704	120.4346
Start date	Jun 2010	Aug 2011	Dec 2011	Nov 2012	Jun 2013	Feb 2018	Nov 2017	Apr 2011
Biology	Eutrophic	Super eutrophic	Submerged macrophyte	Transitional	Mesotrophic	Eutrophic	Aquaculture	Cropland/ Rural residence
Met height (m)	3.5	8.0	8.5	9.4	8.5	6.0	4.5	10.0
T _w / T _s depths (cm)	20, 50, 100, 150, sediment	20, 50, 100, 150, sediment	20, 50, 100, 150, sediment	20, 50, 100, 150, sediment	20, 50, 100, 150, sediment	20, 50, 100, 150, sediment	20, 50, sediment	5, 10, 20
Radiation height (m)	1.5	1.5	1.5	1.5	1.5	1.5	1.5	3.0
EC height (m)	3.5	8.5	8.5	9.4	8.5	6.0	4.5	20

336

337



338

339 **Table 2.** Percent of data coverage

Variable type	MLW	DPK	BFG	XLS	PTS	DTH	MLW2	DS
Micrometeorology	93.3	81.1	97.6	97.0	97.5	98.1	90.3	91.7
Radiation flux	85.5	90.8	96.9	97.4	98.6	98.2	98.2	82.7
Water/soil temperature	83.4	81.3	94.0	91.1	90.3	87.7	22.4	98.4
Eddy flux	73.3	61.8	82.7	79.1	80.6	85.7	85.5	82.8

340

341

342

343



344

345 **Table 3.** A list of data quality flags

Flag	Data quality description
0	Original data
1	Gap-filled with time interpolation
2	Gap-filled with spatial interpolation
3	Gap-filled with bulk relationship
4	NAN

346

347



348

349 **Table 4.** A list of data columns and variable definitions

Column	Description	Variable name	Unit
1	Year	Year	–
2	Month	Month	–
3	Day	Day	–
4	Hour	HH	–
5	Minute	MM	–
6	Day of Year	DOY	–
7	Air pressure	P	kPa
8	Quality flag of air pressure	P_flag	
9	Air temperature	Ta	°C
10	Quality flag of air temperature	Ta_flag	
11	Relative humidity	RH	%
12	Quality flag of Relative humidity	RH_flag	
13	Wind speed	WS	m s ⁻¹
14	Quality flag of wind speed	WS_flag	
15	Wind direction	WD	Degree
16	Quality flag of wind direction	WD_flag	
17	Rainfall	R	mm
18	Quality flag of rainfall	R_flag	
19	Upward shortwave radiation	UR	W m ⁻²
20	Quality flag of upward shortwave radiation	UR_flag	
21	Downward shortwave radiation	DR	W m ⁻²
22	Quality flag of downward shortwave radiation	DR_flag	
23	Upward longwave radiation	ULR	W m ⁻²
24	Quality flag of upward longwave radiation	ULR_flag	
25	Downward longwave radiation	DLR	W m ⁻²
26	Quality flag of downward longwave radiation	DLR_flag	
27	Water temperature at 0.2 m	T _{w_20}	°C



28	Quality flag of Water temperature at 0.2 m	T _{w_20_flag}	
29	Water temperature at 0.5 m	T _{w_50}	°C
30	Quality flag of Water temperature at 0.5 m	T _{w_50_flag}	
31	Water temperature at 1.0 m	T _{w_100}	°C
32	Quality flag of Water temperature at 1.0 m	T _{w_100_flag}	
33	Water temperature at 1.5 m	T _{w_150}	°C
34	Quality flag of water temperature at 1.5 m	T _{w_150_flag}	
35	Sediment temperature	T _{w_bot}	°C
36	Quality flag of sediment temperature	T _{w_bot_flag}	
37	Friction velocity	U*	m s ⁻¹
38	Quality flag of friction velocity	U*_flag	
39	Sensible heat flux	H	W m ⁻²
40	Quality flag of sensible heat flux	H_flag	
41	Latent heat flux	LE	W m ⁻²
42	Quality flag of latent heat flux	LE_flag	

350 Notes: 1) Time marks end of an observation in Beijing time (UTC+8:00); 2) At the DS site, columns 27, 29,
 351 and 31 represent soil temperature at 5, 10, and 20 cm, respectively.

352 .

353

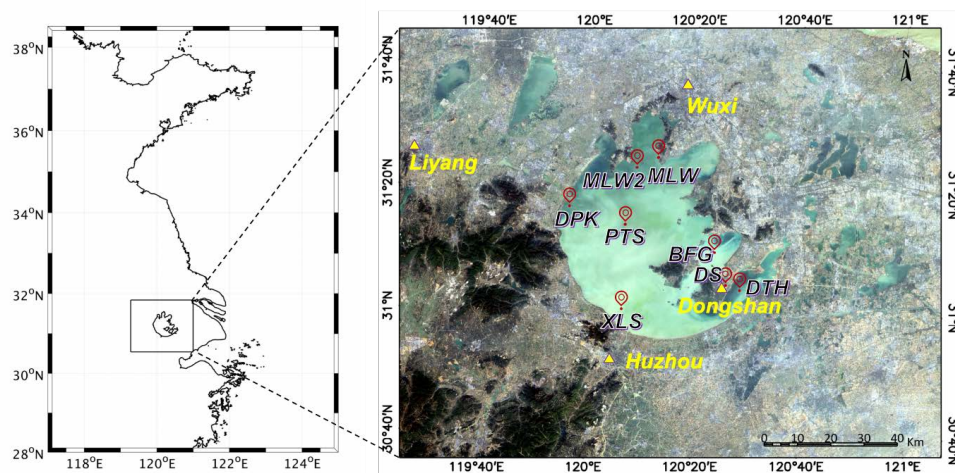
354

355



356

357



358

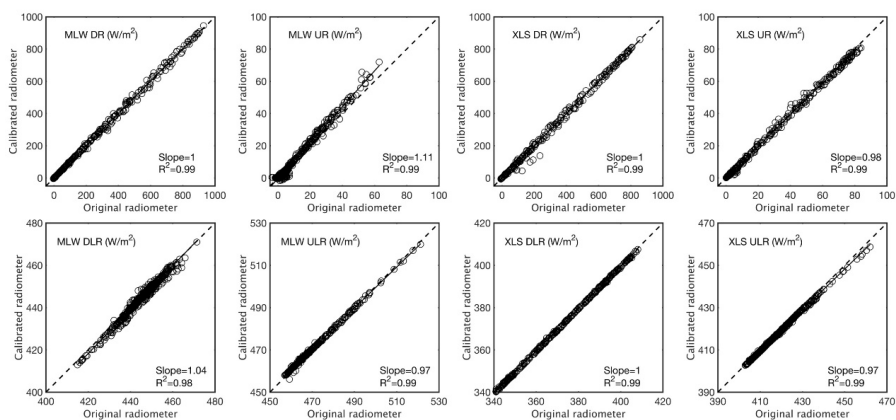
359 **Figure 1.** Map showing locations of Lake Taihu, eddy covariance sites (red bubbles) and
360 WMO weather stations (yellow triangles). The background is a natural color image from
361 LANDSAT 8 without correction for atmospheric interference.

362

363



364
365
366



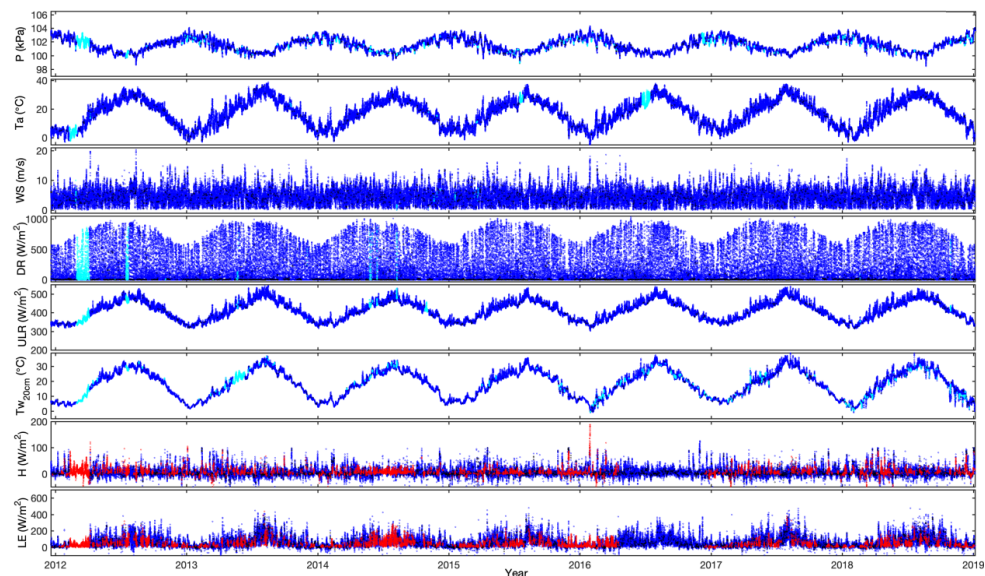
367
368
369
370
371
372

Figure 2. Comparison of four components of the radiation balance between the original radiometer (horizontal axis) and a laboratory standard (vertical axis) at MLW and XLS. Refer to Table 4 for variable definitions.



373

374



375

376 **Figure 3.** Complete gap-filled time series for selected variables observed at BFG. Blue, black,
377 cyan and red dots represent quality flag 0, 1, 2, and 3, respectively. Variable definitions are
378 given in Table 4

379

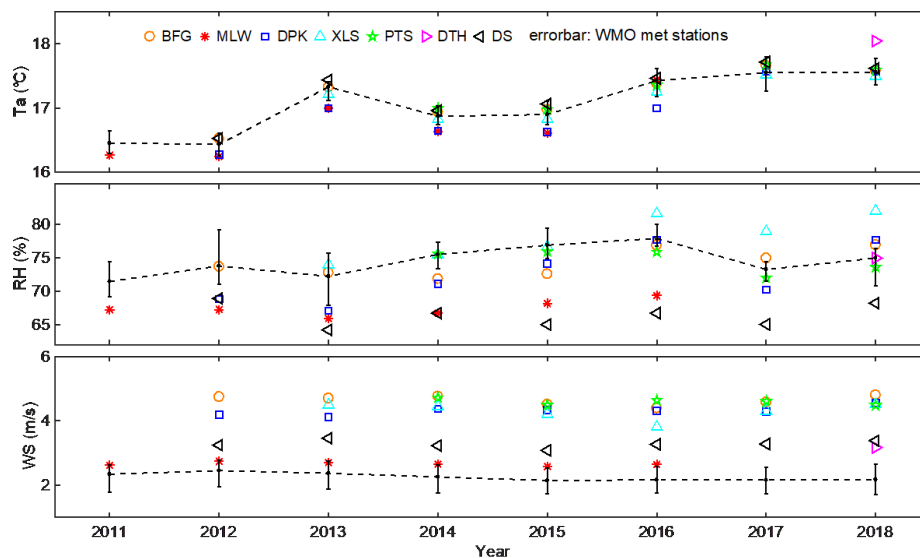
380

381



382

383



384

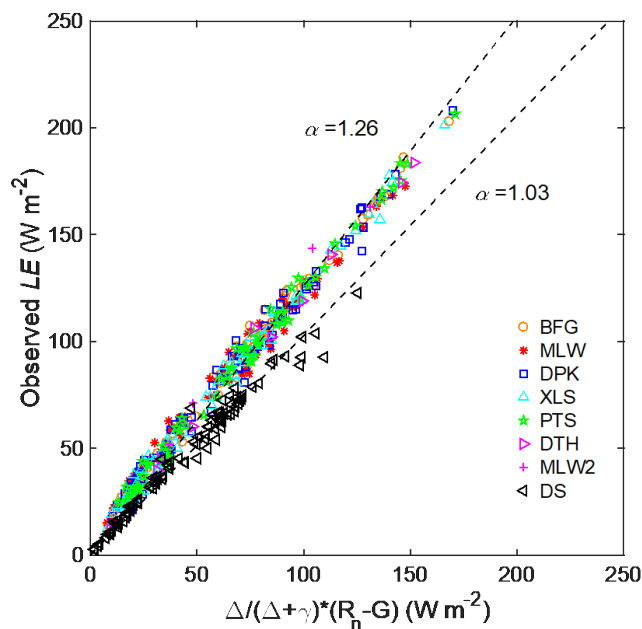
385 **Figure 4.** Annual mean air temperature (top), relative humidity (middle) and wind speed
386 (bottom) observed at the eddy flux sites (symbols) and at the four WMO weather stations
387 around the lake (line). Error bar represents the range of the annual means of the four WMO
388 stations.

389



390

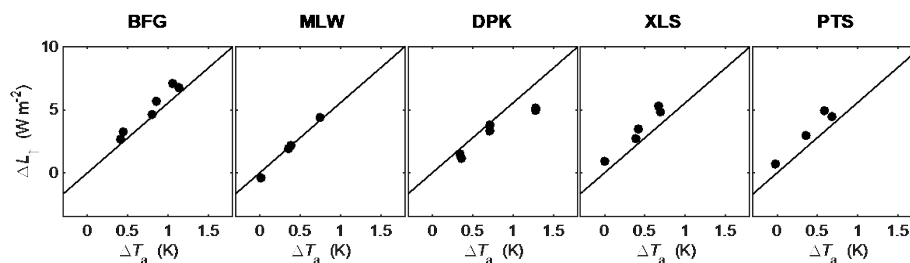
391



392

393 **Figure 5.** Comparison of observed monthly latent heat flux with Priestley-Taylor model
394 prediction using the original α coefficient of 1.26 and a modified coefficient of 1.03. Here
395 R_n is net radiation, G is heat storage in the water column, Δ is the slope of the saturation
396 vapor pressure curve, and γ is the psychrometric constant.

397



398

399 **Figure 6.** The relationship between changes in observed annual mean upward longwave
400 radiation flux and annual mean air temperature (dots). Solid lines represent the prediction of
401 the Stefan-Boltzmann Law.

402



403

404 **References**

- 405 Barr, A. G., King, K. M., Gillespie, T. J., Den Hartog, G. and Neumann, H. H.: A comparison of Bowen ratio
406 and eddy correlation sensible and latent heat flux measurements above deciduous forest, *Boundary-Layer*
407 *Meteorol.*, 71(1–2), 21–41, 1994.
- 408 Blanken, P. D., Black, T. A., Yang, P. C., Neumann, H. H., Nesic, Z., Staebler, R., Den Hartog, G., Novak, M.
409 D. and Lee, X.: Energy balance and canopy conductance of a boreal aspen forest: partitioning overstory and
410 understory components, *J. Geophys. Res. Atmos.*, 102(D24), 28915–28927, 1997.
- 411 Blanken, P. D., Spence, C., Hedstrom, N. and Lenters, J. D.: Evaporation from Lake Superior: 1. Physical
412 controls and processes, *J. Great Lakes Res.*, 37(4), 707–716, doi:10.1016/j.jglr.2011.08.009, 2011.
- 413 Charusombat, U., Fujisaki-Manome, A., Gronewold, A. D., Lofgren, B. M., Anderson, E. J., Blanken, P.,
414 Spence, C., Lenters, J. D., Xiao, C. and Fitzpatrick, L. E.: Evaluating and improving modeled turbulent heat
415 fluxes across the North American Great Lakes, *Hydrol. Earth Syst. Sci.*, 22(10), 2018.
- 416 Deng, B., Liu, S., Xiao, W., Wang, W., Jin, J. and Lee, X.: Evaluation of the CLM4 lake model at a large and
417 shallow freshwater lake, *J. Hydrometeorol.*, 14(2), 636–649, doi:10.1175/JHM-D-12-067.1, 2013.
- 418 Downing, J. A., Prairie, Y. T., Cole, J. J., Duarte, C. M., Tranvik, L. J., Striegl, R. G., McDowell, W. H.,
419 Kortelainen, P., Caraco, N. F., Melack, J. M. and Middelburg, J. J.: The global abundance and size distribution
420 of lakes, ponds, and impoundments, *Limnol. Oceanogr.*, 51(5), 2388–2397, doi:10.4319/lo.2006.51.5.2388,
421 2006.
- 422 Du, Q., Liu, H., Xu, L., Liu, Y. and Wang, L.: The monsoon effect on energy and carbon exchange processes
423 over a highland lake in the southwest of China, *Atmos. Chem. Phys.*, 18(20), 15087–15104, 2018.
- 424 Franz, D., Mammarella, I., Boike, J., Kirillin, G., Vesala, T., Bornemann, N., Larmanou, E., Langer, M. and
425 Sachs, T.: Lake-atmosphere heat flux dynamics of a thermokarst lake in arctic Siberia, *J. Geophys. Res. Atmos.*,
426 123(10), 5222–5239, 2018.
- 427 Franz, D., Mammarella, I., Boike, J., Kirillin, G., Vesala, T., Bornemann, N., Larmanou, E., Langer, M. and
428 Sachs, T.: Lake-atmosphere heat flux dynamics of a thermokarst lake in arctic Siberia, *J. Geophys. Res. Atmos.*,
429 123(10), 5222–5239, 2018.
- 430 Hamdani, I., Assouline, S., Tanny, J., Lensky, I. M., Gertman, I., Mor, Z. and Lensky, N. G.: Seasonal and
431 diurnal evaporation from a deep hypersaline lake: the Dead Sea as a case study, *J. Hydrol.*, 562, 155–167, 2018.
- 432 Hu, C., Wang, Y., Wang, W., Liu, S., Piao, M., Xiao, W. and Lee, X.: Trends in evaporation of a large
433 subtropical lake, *Theor. Appl. Climatol.*, 129(1–2), 159–170, doi:10.1007/s00704-016-1768-z, 2017.
- 434 Lee, X., Massman, W. and Law, B.: *Handbook of micrometeorology: a guide for surface flux measurement and*
435 *analysis*, Springer Science & Business Media., 2004.



- 436 Lee, X., Liu, S., Xiao, W., Wang, W., Gao, Z., Cao, C., Hu, C., Hu, Z., Shen, S., Wang, Y., Wen, X., Xiao, Q.,
437 Xu, J., Yang, J. and Zhang, M.: The taihu eddy flux network: An observational program on energy, water, and
438 greenhouse gas fluxes of a large freshwater lake, *Bull. Am. Meteorol. Soc.*, 95(10), 1583–1594,
439 doi:10.1175/BAMS-D-13-00136.1, 2014.
- 440 Li, Z., Lyu, S., Ao, Y., Wen, L., Zhao, L. and Wang, S.: Long-term energy flux and radiation balance
441 observations over Lake Ngoring, Tibetan Plateau, *Atmos. Res.*, 155, 13–25, 2015.
- 442 Nordbo, A., Launiainen, S., Mammarella, I., Leppäranta, M., Huotari, J., Ojala, A. and Vesala, T.: Long-term
443 energy flux measurements and energy balance over a small boreal lake using eddy covariance technique, *J.*
444 *Geophys. Res. Atmos.*, 116(D2), 2011.
- 445 Subin, Z. M., Riley, W. J. and Mironov, D.: An improved lake model for climate simulations: Model structure,
446 evaluation, and sensitivity analyses in CESM1, *J. Adv. Model. Earth Syst.*, 4(2), 1–27,
447 doi:10.1029/2011MS000072, 2012.
- 448 Tanny, J., Cohen, S., Assouline, S., Lange, F., Grava, A., Berger, D., Teltch, B. and Parlange, M. B.:
449 Evaporation from a small water reservoir: Direct measurements and estimates, *J. Hydrol.*, 351(1–2), 218–229,
450 2008.
- 451 Twine, T. E., Kustas, W. P., Norman, J. M., Cook, D. R., Houser, Pr., Meyers, T. P., Prueger, J. H., Starks, P. J.
452 and Wesely, M. L.: Correcting eddy-covariance flux underestimates over a grassland, *Agric. For. Meteorol.*,
453 103(3), 279–300, 2000.
- 454 Verpoorter, C., Kutser, T., Seekell, D. A. and Tranvik, L. J.: A global inventory of lakes based on
455 high-resolution satellite imagery, *Geophys. Res. Lett.*, 41(18), 6396–6402, doi:10.1002/2014GL060641, 2014.
- 456 Vesala, T., Huotari, J., Rannik, Ü., Suni, T., Smolander, S., Sogachev, A., Launiainen, S. and Ojala, A.: Eddy
457 covariance measurements of carbon exchange and latent and sensible heat fluxes over a boreal lake for a full
458 open-water period, *J. Geophys. Res. Atmos.*, 111(11), 1–12, doi:10.1029/2005JD006365, 2006.
- 459 Wang, B., Ma, Y., Wang, Y., Su, Z. and Ma, W.: Significant differences exist in lake-atmosphere interactions
460 and the evaporation rates of high-elevation small and large lakes, *J. Hydrol.*, 573, 220–234, 2019.
- 461 Wang, W., Xiao, W., Cao, C., Gao, Z., Hu, Z., Liu, S., Shen, S., Wang, L., Xiao, Q., Xu, J., Yang, D. and Lee,
462 X.: Temporal and spatial variations in radiation and energy balance across a large freshwater lake in China, *J.*
463 *Hydrol.*, 511, 811–824, doi:10.1016/j.jhydrol.2014.02.012, 2014.
- 464 Wang, Y., Gao, Y., Qin, H., Huang, J., Liu, C., Hu, C., Wang, W., Liu, S. and Lee, X.: Spatiotemporal
465 Characteristics of Lake Breezes over Lake Taihu, China, *J. Appl. Meteorol. Climatol.*, 56(7), 2053–2065, 2017.
- 466 Webb, E. K., Pearman, G. I. and Leuning, R.: Correction of flux measurements for density effects due to heat
467 and water vapour transfer, *Q. J. R. Meteorol. Soc.*, 106(447), 85–100, 1980.
- 468 Wilson, K., Goldstein, A., Falge, E., Aubinet, M., Baldocchi, D., Berbigier, P., Bernhofer, C., Ceulemans, R.,



- 469 Dolman, H. and Field, C.: Energy balance closure at FLUXNET sites, *Agric. For. Meteorol.*, 113(1–4), 223–243,
470 2002.
- 471 Xiao, K., Griffis, T. J., Baker, J. M., Bolstad, P. V., Erickson, M. D., Lee, X., Wood, J. D., Hu, C. and Nieber, J.
472 L.: Evaporation from a temperate closed-basin lake and its impact on present, past, and future water level, *J.*
473 *Hydrol.*, 561, 59–75, 2018.
- 474 Xiao, W., Liu, S., Wang, W., Yang, D., Xu, J., Cao, C., Li, H. and Lee, X.: Transfer Coefficients of Momentum,
475 Heat and Water Vapour in the Atmospheric Surface Layer of a Large Freshwater Lake, *Boundary-Layer*
476 *Meteorol.*, 148(3), 479–494, doi:10.1007/s10546-013-9827-9, 2013.
- 477 Xiao, W., Liu, S., Li, H., Xiao, Q., Wang, W., Hu, Z., Hu, C., Gao, Y., Shen, J., Zhao, X., Zhang, M. and Lee,
478 X.: A flux-gradient system for simultaneous measurement of the CH₄, CO₂, and H₂O fluxes at a lake-air
479 interface, *Environ. Sci. Technol.*, 48(24), 14490–14498, doi:10.1021/es5033713, 2014.
- 480 Xu, J., Lee, X., Xiao, W., Cao, C., Liu, S., Wen, X., Xu, J., Zhang, Z. and Zhao, J.: Interpreting the ¹³C/¹²C ratio
481 of carbon dioxide in an urban airshed in the Yangtze River Delta, China, *Atmos. Chem. Phys.*, 17(5),
482 doi:10.5194/acp-17-3385-2017, 2017.
- 483 Yusup, Y. and Liu, H.: Effects of Atmospheric Surface Layer Stability on Turbulent Fluxes of Heat and Water
484 Vapor across the Water–Atmosphere Interface, *J. Hydrometeorol.*, 17(11), 2835–2851, 2016.
- 485 Zhang, M., Xiao, Q., Zhang, Z., Gao, Y., Zhao, J., Pu, Y., Wang, W., Xiao, W., Liu, S. and Lee, X.: Methane
486 flux dynamics in a submerged aquatic vegetation zone in a subtropical lake, *Sci. Total Environ.*, 672,
487 doi:10.1016/j.scitotenv.2019.03.466, 2019a.
- 488 Zhang, X., Huang, J., Li, G., Wang, Y., Liu, C., Zhao, K., Tao, X., Hu, X.-M. and Lee, X.: Improving
489 Lake-Breeze Simulation with WRF Nested LES and Lake Model over a Large Shallow Lake, *J. Appl. Meteorol.*
490 *Climatol.*, 58(8), 1689–1708, 2019b.
- 491 Zhang, Z., Zhang, M., Cao, C., Wang, W., Xiao, W., Xie, C., Chu, H., Wang, J., Zhao, J., Jiayu, Jia, L., Liu, Q.,
492 Huang, W., Zhang, W., Lu, Y., Xie, Y., Wang, Y., Pu, Y., Hu, Y., Chen, Z., Qin, Z. and Lee, X.: A dataset of
493 microclimate and radiation and energy fluxes from the Lake Taihu Eddy Flux Network, *Harvard Dataverse*,
494 <https://doi.org/10.7910/DVN/HEWCWM>, 2020
- 495 Zhao, X. and Liu, Y.: Variability of surface heat fluxes and its driving forces at different time scales over a large
496 ephemeral lake in China, *J. Geophys. Res. Atmos.*, 123(10), 4939–4957, 2018.
- 497